THE JOURNAL OF PHYSICAL CHEMISTRY B
A JOURNAL OF THE AMERICAN CHEMICAL SOCIETY

pubs.acs.org/JPCB

Article

Understanding Solute-Hydrotrope Aggregation in Aqueous Solutions: A Molecular Dynamics Approach

Published as part of The Journal of Physical Chemistry B special issue "Athanassios Z. Panagiotopoulos Festschrift".

Esteban Cea-Klapp, Dinis O. Abranches, Eliseo Marin-Rimoldi, Nicolás F. Gajardo-Parra, Roberto I. Canales, José Matías Garrido, and Edward J. Maginn*

Cite This: https://doi.org/10.1021/acs.jpcb.5c01542

Read Online

ACCESS | Metrics & More | Article Recommendations | Supporting Information

Downloaded via UNIV VIGO on May 9, 2025 at 11:15:32 (UTC).
See https://pubs.acs.org/sharingguidelines for options on how to legitimately share published articles.

ABSTRACT: Hydrotropy is a phenomenon where an amphiphilic molecule (i.e., the hydrotrope) is able to enhance the aqueous solubility of a hydrophobic solute. Understanding the molecular mechanisms behind this phenomenon is crucial to designing new hydrotropes aimed at enhancing the aqueous solubility of specific target solutes. This study investigates the hydrotropic behavior of 1,2-alkanediols in enhancing the aqueous solubility of syringic acid using molecular dynamics (MD) simulations. The analysis carried out here employs several computational methods, including Kirkwood−Buff integrals, solvation free energies, radial distribution functions, and hydrogen bonding number. The solvation free energy results reported in this work help explain the thermodynamic favorability of syringic acid solubilization in the presence of 1,2-alkanediols, aligning with experimental trends. In addition, MD simulations reveal a pronounced affinity between syringic acid and 1,2-alkanediols, particularly at low hydrotrope concentrations. This high affinity is driven by the alkyl chain of each hydrotrope when water is the main solvent, resulting in an increase in the solubility of the solute as the length of the hydrotrope alkyl chain increases. However, a shift in the solubilization mechanism is seen when water is no longer the main solvent, with the hydrogen bonding capabilities of the hydrotrope playing a larger role than its alkyl chains. Under low water concentration conditions, longer alkyl chains in the hydrotrope have difficulty forming hydrogen bonds, leading to an opposite trend compared to lower hydrotrope concentrations. This different behavior with composition results in a maximum solubility for systems with long alkyl chains at intermediate hydrotrope concentrations.

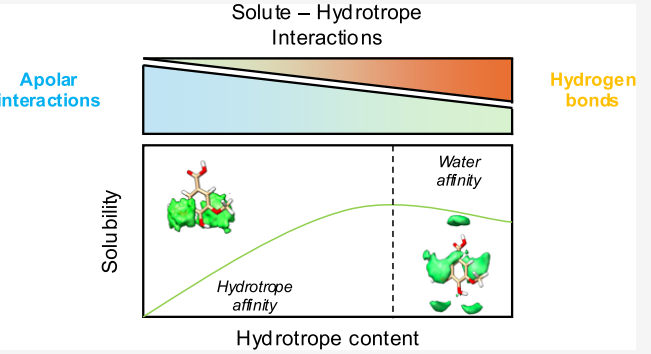

INTRODUCTION

The term "hydrotrope" and its extension, "hydrotropy", were proposed more than a century ago by Carl Neuberg.[1,2] Hydrotropy refers to a phenomenon in which the solubility of hydrophobic compounds in water is increased by adding an amphiphilic molecule known as a hydrotrope.[3] This process differs from other solubilization techniques, such as micelle formation and emulsification, because hydrotropes exhibit weak aggregation in solution without a hydrophobic solute.[4] Owing to their ability to enhance the aqueous solubility of any type of hydrophobic solute, hydrotropes have a wide range of applications, including the separation of near-boiling compounds, the enhancement of heterogeneous chemical reactions, the extraction of natural products, and the improvement of drug solubilization.[5] Understanding the molecular mechanisms underlying this process is essential to designing novel hydrotropes, optimizing the solubilization processes of poorly soluble compounds, and finding the best solute-hydrotrope combinations for target applications.

There are several examples of hydrotropes in the literature that illustrate their versatility and effectiveness.[5] However, researchers are progressively focusing on biobased compounds as efficient hydrotropes, avoiding the use of hazardous or nonsustainable options.[6] Dihydrolevoglucosenone, commonly known as "cyrene", is a biodegradable solvent derived from cellulose waste that has demonstrated significant potential as a hydrotrope by increasing the solubility of pharmacologically relevant compounds up to 100-fold.[7,8] In aqueous solutions,

Received: March 6, 2025
Revised: April 27, 2025
Accepted: April 29, 2025

ACS Publications © XXXX American Chemical Society

cyrene establishes a chemical equilibrium between its diol and ketone forms, with the ketone form being primarily responsible for this remarkable solubility enhancement.[9] In addition, other biobased compounds such as glycerol ethers and alkanediols have been shown to enhance the solubility of phenolic compounds such as ferulic acid, gallic acid, and syringic acid in water.[10−12] Different ionic liquids (ILs) have been studied as hydrotropes to enhance the aqueous solubility of drugs, such as ibuprofen,[13] artemisinin,[14,15] and naproxen,[13] or to improve the extraction of biomolecules, including vanillin and gallic acid.[16] Recently, deep eutectic solvents (DESs) based on choline chloride have been explored as hydrotropes to enhance the solubility of lignin.[17] These examples underscore the diverse chemical nature of hydrotropes and the importance of understanding their underlying molecular mechanisms to innovate and improve solubilization processes.

The mechanism behind hydrotropy is not entirely understood, and various hypotheses have been proposed to explain this phenomenon.[5] One such hypothesis suggests that hydrotropes experience self-aggregation in aqueous solution above a particular concentration, known as the minimum hydrotropic concentration (MHC), similar to the critical micelle concentration (CMC) for surfactants.[18−22] Another hypothesis proposes that hydrotropes disrupt the "water structure", acting as chaotropic agents that weaken the hydrophobic effect and thus increase solubility.[23,24] A third hypothesis involves the hydrotrope molecule that forms complexes with the solute in specific stoichiometric ratios.[25,26] Although molecular dynamics (MD) simulations have been employed to support some of these ideas,[27−30] they remain inconclusive from the perspective of statistical thermodynamics.[31,32] Instead, the cooperativity theory of hydrotropy has gained support through the fluctuation theory of solution[33] and experimental validation by ^{1}H NMR chemical shifts.[34] This theory proposes that enhanced solubility results from the cooperative clustering of hydrotrope molecules around the solute, driven by strong hydrophobic interactions between their apolar moieties.[34] This clustering behavior has also been observed in MD simulations, which have attempted to provide support for other hypotheses as well.[27−30]

Considering that hydrotropy depends on the apolar volumes of both the solute and hydrotrope, compound families with adjustable apolarity are useful for understanding this phenomenon and designing green hydrotropes for specific uses. There are a few studies in the literature that have investigated this, such as those involving monoglycerol ethers and alkanediols with varying alkyl side chain sizes.[11,12,34] These studies reveal that the solubility enhancement of a solute correlates well with the apolarity of the hydrotrope. These works support the cooperativity theory of hydrotropy, showing that the hydrophobic nature of the hydrotrope is a key factor in the solubility enhancement, especially in the dilute region. Interestingly, these studies also show that the extent of solute-hydrotrope aggregation reaches a maximum when the apolar surface areas of the hydrotrope and solute match.

Among these studies, the investigation of 1,2-alkanediols as hydrotropes increasing the aqueous solubility of 4-hydroxy-3,5-dimethoxybenzoic acid ("syringic acid")[12] presents particularly compelling results, which are illustrated in Figure 1. First, at low concentrations of hydrotrope (until a hydrotrope mole fraction of 0.1), the enhancement in the solubility of syringic acid is significantly influenced by the length of the hydrotrope alkyl chain; longer alkanediols show better performance.

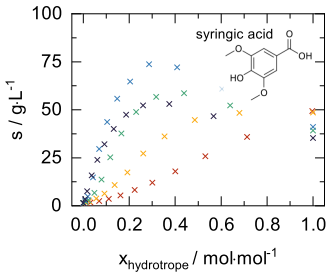

Figure 1. Experimental aqueous solubility of syringic acid as a function of the hydrotrope molar fraction free of solute at 303.2 K.[12] Hydrotropes: 1,2-ethanediol (×), 1,2-propanediol (×), 1,2-butanediol (×), 1,2-pentanediol (×), and 1,2-hexanediol (×). Adapted with permission from Abranches et al.[12] Copyright 2022 Royal Society of Chemistry.

Second, for intermediate concentrations of hydrotrope (between hydrotrope mole fractions of 0.1 and 0.6) there is an optimal alkyl chain length, which is that of 1,2-pentanediol. Third, at high hydrotrope concentrations (above hydrotrope mole fractions of 0.6), the system experiences a reduction in solubility efficiency, leading to lower solubility as more hydrotrope is added. The first two findings align with the cooperativity theory of hydrotropy[33] and the concept of hydrophobic interactions driving the accumulation of hydrotropes around the solute. However, the decrease in solubility does not match the typical sigmoidal curve, where the solubility increases suddenly and then reaches a plateau at higher hydrotrope concentrations when plotted against hydrotrope concentration.

Motivated by these experimental findings, the present study investigates the aqueous solubility behavior of syringic acid with the addition of 1,2-alkanediols using MD simulations to understand the molecular mechanisms across all composition ranges. The first section of this paper outlines the methodology, including the force field and simulation details. Next, a force field validation is provided, considering density data for pure and aqueous binary mixtures of the involved 1,2-alkanediols, binary Kirkwood-Buff integrals (KBI), and solvation free energy for syringic acid. The results section utilizes the Kirkwood-Buff theory and offers a comprehensive analysis of the interactions between solvent molecules and the solute by decoupling them using the radial distribution function (RDF) and spatial distribution function (SDF). These analyses were performed at different concentrations of hydrotropes for the entire family to reveal the distinct mechanisms in each region.

COMPUTATIONAL METHODS

Force Fields. The simulations were carried out using a nonpolarizable force field to describe atomic interactions. Water was modeled using the SPC/E model.[35] Force field parameters for syringic acid and 1,2-alkendiols were determined using the second generation of the General Amber Force Field (GAFF2),[36] facilitated by the AnteChamber PYthon Parser interfacE (ACPYPE).[37,38] Lorentz−Berthelot[39,40] mixing rules were employed to calculate the Lennard−Jones (LJ) parameters for interactions between different atom types. Additionally, the 1−4 LJ and Coulombic interactions were scaled by factors of 0.5 and 0.8333, respectively. Partial atomic charges were assigned using the RESP2 method,[41] which implicitly considers polarization

https://doi.org/10.1021/acs.jpcb.5c01542
J. Phys. Chem. B XXXX, XXX, XXX−XXX

effects. In this method, the structure of each molecule was optimized both in vacuum and in water at the B3LYP/6−311++g(d,p) level of theory. The optimization in water, as an implicit solvent, employed the Polarizable Continuum Model (PCM)[42] with the integral equation formalism variant (IEFPCM).[43] Final partial charges were obtained by taking the average of those values between the condensed phase and vacuum (this is referred to as RESP2$_{0.5}$). All quantum mechanical optimizations were performed using the Gaussian 16 package.[44] Initial molecular structures were sourced from the PubChem database. A good charge distribution method, such as RESP2, can provide a force field that yields better estimates of free energies and Kirkwood-Buff integrals (KBIs), which are useful for accurate solvation analysis.[45,46] The molecular parameters can be found in the GitHub repository of this work at https://github.com/MaginnGroup/syringic_acid_KBI.

Simulations Details. The simulations were performed using GROMACS 2022.1.[47,48] A time step of 1 fs was used in which the equations of motion were integrated with the leapfrog algorithm.[49] A cutoff of 1.2 nm for both Coulomb and LJ interactions was used. Long-range electrostatic interactions were treated using the particle mesh Ewald method.[50] Analytical dispersion corrections were applied to both energy and pressure. The LINCS algorithm was utilized to constrain the bonds that involve hydrogen atoms.[51] All initial configurations were created using PACKMOL[52] and then the configuration was energy minimized using the steepest descent algorithm. Equilibration was carried out for 5 ns using the v-rescale thermostat[53] with a time constant of 1 ps and the Berendsen barostat[54] with a time constant of 2 ps. For the production phase, the Nosé-Hoover thermostat[55,56] with a time constant of 1 ps and the Parrinello−Rahman barostat[57,58] with a time constant of 2 ps were used.

Details on the number of molecules and simulation times for the binary systems (hydrotrope + water) and the ternary systems (solute + hydrotrope + water) can be found in Table S1.

Kirkwood−Buff Integrals. The Kirkwood-Buff theory of solution explores the fluctuations in the grand canonical ensemble and their connection to macroscopic properties.[59] These properties include derivatives of chemical potentials with respect to concentrations, partial molar volumes, and isothermal compressibility for any number of components.[60] The theory expresses these macroscopic properties through integrals of RDFs for different molecular pairs in the solution. The key parameter in these relations is the KBI, denoted as G_{ij}^{∞}, defined by eq 1,

$$G_{ij}^{\infty} \equiv \int_0^{\infty} 4\pi r^2 [g_{ij}^{\infty}(r) - 1] dr \tag{1}$$

where r represents the center-of-mass distance between particles, and $g_{ij}^{\infty}(r)$ is the RDF for species i and j in an infinite volume in the grand canonical ensemble.

It should be stressed that the KBI can be interpreted as a measure of the affinity between pairs of molecule types.[61] A large G_{ij}^{∞} value indicates an overall attraction between the two species, which can be thought of as an excess of molecules of one species around the other in relation to the molecules in the bulk phase.

Computing KBIs using eq 1 poses significant challenges due to the necessity of integrating to infinity, while MD simulations are inherently limited by finite system sizes.[62] Simple truncation of the integral can lead to poor convergence, making accurate estimation difficult. To address this issue, the Krüger correction[63] was applied. This correction defines a finite-size KBI (G_{ij}^{V}), which for a spherical geometry of diameter L is defined by eq 2

$$G_{ij}^{V}(L) = \int_0^{L} 4\pi r^2 [g_{ij}^{\infty}(r) - 1]\left(1 - \frac{3}{2}\left(\frac{r}{L}\right) + \frac{1}{2}\left(\frac{r}{L}\right)^3\right) dr \tag{2}$$

To estimate the KBI for an infinite system, the finite-size KBI can be extrapolated to $L \to \infty$ using its linear behavior with $1/L$ at long distances. The extrapolation was performed systematically within the range $L = 4\sigma_{ij}$ to $8\sigma_{ij}$, where σ_{ij} is the distance at which $g_{ij}(r)$ first becomes nonzero. Despite the application of this correction, the simulations required substantial computational resources, including large cubic boxes (>7 nm) and long simulation times (>50 ns in some cases), to ensure adequate sampling and accuracy. Error estimation was conducted by performing three independent simulations for each system to reduce the uncertainty associated with a single simulation.

Solvation Free Energy. The solvation free energy of syringic acid was computed using separate MD simulations. The initial configurations consisted of one molecule of syringic acid and 2500 solvent molecules, comprising a mixture of hydrotrope and water at the desired molar composition. These configurations were energy-minimized using the same protocol as in the previous section. Equilibration was carried out using the stochastic dynamics integrator and the Parrinello−Rahman barostat for 10 ns. Following equilibration, the Hamiltonian Replica Exchange (HREX) method,[64] implemented in GROMACS,[65] was used for 20 ns.

The HREX method connects the state where the solute is fully interacting with the solvents with the state where the intermolecular interactions of the solute molecule with the system are turned off. To ensure sufficient phase-space overlap among adjacent states, the two terminal states were linked using 22 alchemical intermediate states, gradually reducing the interactions between the solute molecule and the rest of the system. The 24 configurations were swapped based on the Metropolis criterion every 2000 steps,[66] with 10,000 attempted exchanges performed for each swap. The potential energy was dependent on the coupling parameter λ, which ranged from 0 (interactions on) to 1 (interactions off). First, the electrostatic interactions of the solute with the environment were turned off (λ_{Coul} = 0.0, 0.05, 0.10, 0.15, 0.20, 0.30, 0.40, 0.60, 0.80, 1.0), followed by the LJ parameters of the solute to zero (λ_{LJ} = 0.0, 0.10, 0.20, 0.30, 0.40, 0.45, 0.50, 0.55, 0.60, 0.65, 0.70, 0.80, 0.90, 0.95, 1.0). To avoid singularities and numerical instabilities during the decoupling of interactions, a soft core potential was used for LJ interactions.[67]

The postprocessing to compute the solvation free energy was done using the multistate Bennett acceptance ratio (MBAR) estimator,[68] implemented in the open software Alchemical Analysis.[69]

RESULTS AND DISCUSSION

Force Field Validation. Due to GAFF2 not being parametrized using the RESP2 methodology, validation is necessary. Figure 2A shows the density for pure hydrotropes at temperatures between 280 and 360 K and atmospheric pressure. The simulation results using the GAFF2/RESP2$_{0.5}$

https://doi.org/10.1021/acs.jpcb.5c01542
J. Phys. Chem. B XXXX, XXX, XXX−XXX

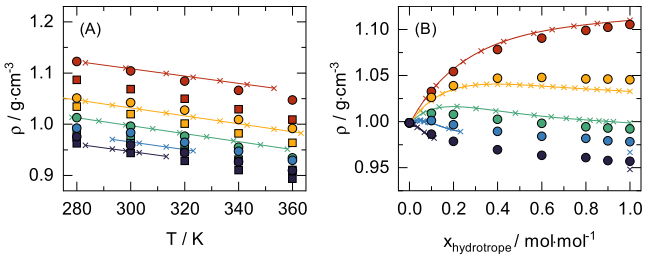

Figure 2. Density at atmospheric pressure for (A) pure hydrotropes at different temperatures and (B) hydrotrope-water mixtures at varying molar fractions at 298.2 K. Comparison between experimental data from the literature (crosses, with fitted lines) and MD results using GAFF2/RESP2$_{0.5}$ without Lennard-Jones scaling (squares), and GAFF2/RESP2$_{0.5}$ with a scaling factor of $f\sigma_{OH}$ = 0.98 (circles). Hydrotropes: 1,2-ethanediol (●),[70,71] 1,2-propanediol (●),[72,73] 1,2-butanediol (●),[74,75] 1,2-pentanediol (●),[76,77] and 1,2-hexanediol (●).[78,79]

force field (squares) indicate an underestimation of the density, which decreases with longer alkyl chain lengths (see Table S2). This suggests that while intermolecular interactions of the alkyl chains are reasonably well described by the force field parameters, the intermolecular interactions of hydroxy groups could be improved. To do this, the LJ size parameters (σ) of the oxygens and hydrogens in the hydroxy groups were scaled by a factor of $f_{\sigma_{OH}}$ = 0.98. Figure 2A,B show that the modified force fields reproduce the experimental densities of the pure hydrotropes at all temperatures studied (circles) and their binary mixtures at 298.2 K very well. This force field modification was applied in the subsequent MD simulation results.

The force field was further validated by computing KBIs from MD simulations and comparing them to KBIs derived from experimental density and vapor−liquid equilibrium measurements[71,73,80−82] using the KBI inversion technique.[61] Figure 3 shows a comparison with the only two binary systems

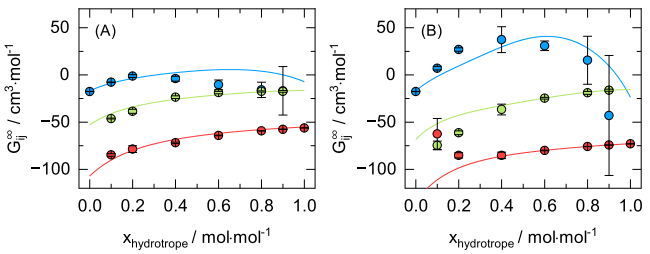

Figure 3. Kirkwood-Buff integrals water−water (●), water-hydrotrope (●), and hydrotrope-hydrotrope (●) for (A) 1,2-ethanediol + water, and (B) 1,2-propanediol + water at 298.2 K and atmospheric pressure. Comparison between experimental inversion (lines) and MD calculations (circles).

for which experimental data are available in the literature for the KBI inversion technique: 1,2-ethanediol + water and 1,2-propanediol + water. The force field qualitatively reproduces the trends among the three KBI pair combinations in both systems. Additionally, it captures the behavior with respect to hydrotrope composition. Notably, the KBIs for hydrotrope-hydrotrope and hydrotrope-water interactions coincide quantitatively with experimental data across the entire composition range for the 1,2-ethanediol system. However, for the binary system with 1,2-propanediol, there is a noticeable overprediction of the hydrotrope-hydrotrope KBI and an underprediction of the hydrotrope-water KBI only at low hydrotrope concentrations. Although finding a force field that accurately predicts KBIs without using them in parametrization is challenging, the results generally agree well with experimental KBI values.

In addition to force field validation, Figure 3 provides insight into the behavior of the hydrotrope-water binary mixtures of the present study. Experimentally, the KBIs for hydrotrope-hydrotrope and hydrotrope-water increase monotonically with the addition of hydrotrope; the increase is greatest at low hydrotrope concentrations. The sharp increase in that region is related to the disruption of water−water hydrogen bond connectivity, which is progressively replaced by water-hydrotrope hydrogen bonds.[82] Additionally, the KBI for hydrotrope-water is consistently larger than that for hydrotrope-hydrotrope across the entire composition range, indicating that hydrotropes are preferentially solvated by water molecules. This preferential solvation is more closely related to the smaller excluded volume in the KBI contribution for hydrotrope-water rather than to stronger interactions between them. Similar conclusions have been reported in the literature for other polyhydroxy alcohols, such as 1,3-propanediol and glycerol, where experimental data are available.[83] Furthermore, both systems exhibit a region where the KBI for water−water interactions reaches a maximum, which can also be observed in the MD simulations. However, these maxima are not sufficiently pronounced compared to those reported for systems with microheterogeneity, such as aqueous solutions of monohydroxy alcohols.[84] Additionally, no maximum is observed in the solute−solute KBI, which would indicate microheterogeneity characterized by self-clustering of water and solute molecules near phase separation, as described in the literature.[84]

The calculation of solvation free energies can be connected with solubility data in a quantitative way, providing numerical values that correlate with the amount of solute that can be dissolved in a solvent. This quantitative connection is more straightforward for solutes with poor solubility, where the solvation free energy calculation at infinite dilution can be assumed to be equal in the thermodynamic limit.[85,86] Nevertheless, the solvation free energy calculation at infinite dilution can qualitatively indicate the thermodynamic favorability of solvation, revealing trends in solute−solvent interactions across different solvents or solvent mixtures. Figure 4 illustrates the solvation free energy of syringic acid in different hydrotrope mixtures. As shown in Figure 4A, increasing the length of the alkyl chain in the hydrotrope at a 10% molar composition leads to a more negative solvation free energy, indicating enhanced thermodynamic favorability for the solvation of syringic acid by the respective solvent. Furthermore, Figure 4B demonstrates that an increase in hydrotrope content in the 1,2-butanediol and water mixture produces an optimal condition beyond which further addition of hydrotrope does not improve the thermodynamic favorability of the solute. These findings align qualitatively with the experimental trends reported in the solubility data.

Kirkwood−Buff Integrals Analysis. The quantification of KBIs for each molecular interaction pair in a solution aids in connecting molecular structure to thermodynamic properties, including chemical potential derivatives.[87] For a solute (e.g., syringic acid) with poor solubility in a solvent (e.g., water) modeled at infinite dilution, the change in its chemical

https://doi.org/10.1021/acs.jpcb.5c01542
J. Phys. Chem. B XXXX, XXX, XXX−XXX

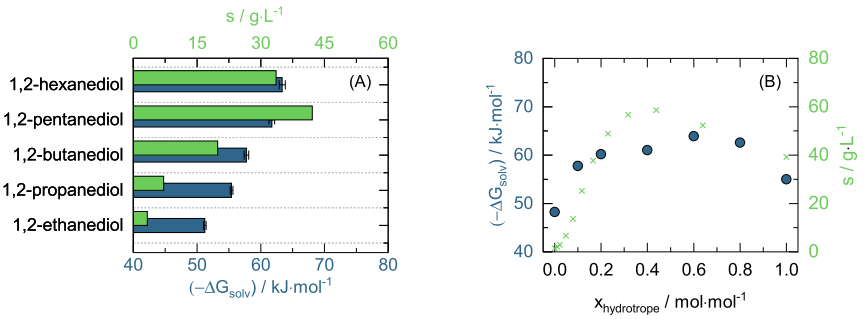

Figure 4. Solvation free energy from MD (ΔG_{solv}) and experimental solubility (s) of syringic acid at 303.2 K in (A) various hydrotrope + water mixtures with 10% hydrotrope concentration, and (B) 1,2-butanediol with varying hydrotrope content.

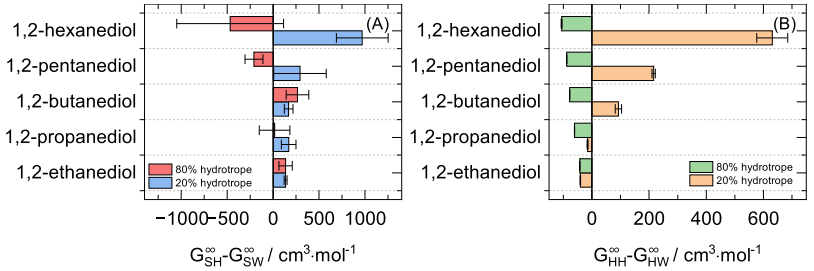

Figure 5. Difference between the Kirkwood−Buff integrals for (A) syringic acid − hydrotrope (G^{∞}_{SH}) and syringic acid − water (G^{∞}_{SW}), and (B) hydrotrope − hydrotrope (G^{∞}_{HH}) and hydrotrope − water (G^{∞}_{HW}), in various hydrotrope + water mixtures at 303.2 K.

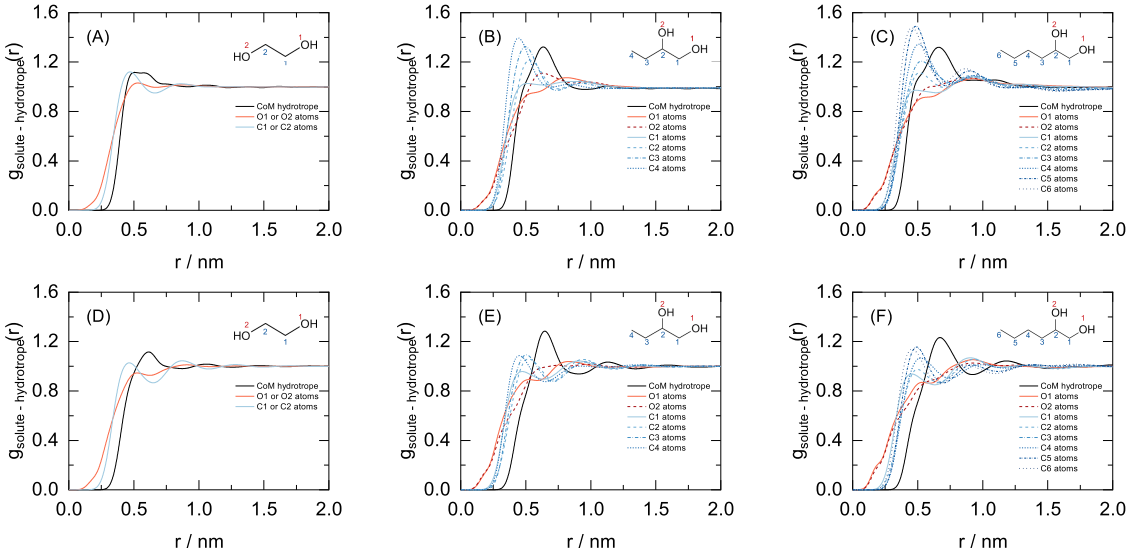

Figure 6. Radial distribution function between the center of mass of syringic acid and the center of mass (CoM) of the hydrotrope or specific atoms for various hydrotrope mole percentage: (A) 20% 1,2-ethanediol, (B) 20% 1,2-butanediol, (C) 20% 1,2-hexanediol, (D) 80% 1,2-ethanediol, (E) 80% 1,2-butanediol, (F) 80% 1,2-hexanediol.

potential upon the addition of a third component (hydrotrope) depends only on four specific KBIs,[87,88] as shown in eq 3,

$$-\frac{1}{RT}\left(\frac{\partial \mu_S}{\partial \rho_H}\right)_{T,P,\rho_S \to 0} = \frac{G^{\infty}_{SH} - G^{\infty}_{SW}}{1 + \rho_H(G^{\infty}_{HH} - G^{\infty}_{HW})} \quad (3)$$

where R is the ideal gas constant, T is the absolute temperature, P is the pressure, μ_i is the chemical potential and ρ_i is the molar concentration. The subscripts represent the components of the ternary mixture: water (W), solute (S), and hydrotrope (H).

Due to the constant composition in eq 3, the derivative of the chemical potential of the solute at infinite dilution is equal to the derivative of its residual chemical potential (often referred to as the solvation free energy). Therefore, changes in the chemical potential of the solute can be linked to changes in its solvation free energy and, consequently, its solubility. If the chemical potential of the solute in the liquid phase decreases (negative derivative), the solubility increases. According to eq 3, the primary factor that increases solubility with the addition of a hydrotrope is the higher affinity of the solute for the hydrotrope compared to water molecules, which is indicated by $G^{\infty}_{SH} > G^{\infty}_{SW}$. Additionally, if the hydrotrope exhibits stronger self-interaction compared to its interaction with water, i.e., G^{∞}_{HH}

https://doi.org/10.1021/acs.jpcb.5c01542
J. Phys. Chem. B XXXX, XXX, XXX−XXX

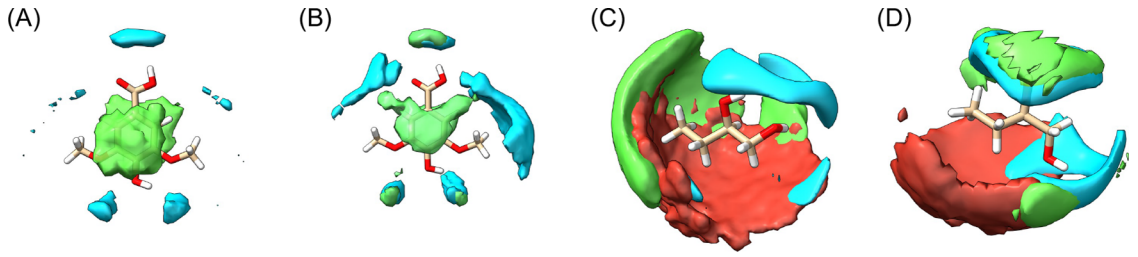

Figure 7. Spatial distribution function for: (A) syringic acid at 20% 1,2-butanediol, (B) syringic acid at 80% 1,2-butanediol, (C) 1,2-butanediol at 20% 1,2-butanediol, and (D) 1,2-butanediol at 80% 1,2-butanediol. Colors: water (●), 1,2-butanediol (●), and syringic acid (●).

> G^{∞}_{HW}, this will decrease the solubility-enhancing effect of the hydrotrope.

Figure 5 illustrates the two main factors influencing solubility, as determined through KBI analysis for the investigated systems. As shown in Figure 5A, at a molar composition of 20% hydrotrope, all systems demonstrate that the solute has a higher affinity for the hydrotrope than for water. This affinity increases with the length of the alkyl chain, following the trend with the Setschenow constants reported by Abranches et al.,[12] which quantify the enhancement of syringic acid solubility in dilute aqueous solutions of hydrotrope. However, at a molar composition of 80%, this affinity decreases and even shifts toward the water molecule for longer alkyl chains. Even though this analysis is at infinite dilution, which is far from the solubility limit for high hydrotrope content, these affinity changes qualitatively match the experimental solubility changes. On the other hand, Figure 5B shows that at low hydrotrope content, the self-aggregation of the hydrotrope increases with the length of the alkyl chain, which is probably an overprediction related to the inaccuracy of the force field in that region, as discussed in the previous section. At high hydrotrope content, there is no self-aggregation, and all the systems look similar, indicating that this is not a major factor in the differences in observed solubility. Figure S1 accounts for the self-aggregation in the denominator of eq 3, and clearly, at high hydrotrope content, all systems look similar to a positive value lower than 1. This indicates that the main term, (G^{∞}_{SH}−G^{∞}_{SW}), is highlighted in the same way in all cases and should not be a major factor in the observed differences in solubility at this hydrotrope content.

Radial and Spatial Distribution Function Analysis. Figures 6 (for 1,2-ethanediol, 1,2-propanediol, and 1,2-hexanediol) and S2 (for 1,2-propanediol and 1,2-pentanediol) present the RDFs for hydrotrope-solute pairs at 20% and 80% molar compositions of hydrotrope. In both cases, the prominent peak in the RDFs between the centers of mass is primarily due to interactions involving atoms in the alkyl chains of the hydrotropes rather than in the hydroxyl groups. Additionally, when the carbon atoms are farther from the polar functional groups (or, in other words, when the carbon atoms are more apolar), the intensity of the peaks increases and these peaks are positioned closer to the center of mass of the solute. The intensity of these peaks also increases with the length of the alkyl chain at a given composition but decreases with increasing hydrotrope concentration. These observations support the hypothesis that hydrophobic interactions between the nonpolar regions of both the solute and the hydrotrope drive the clustering of hydrotrope molecules around the solute.[34] Furthermore, when water is not the main solvent in the system, these interactions decrease, signaling a change in solvation mechanism.[9,12]

The features shown in the RDFs are clearly illustrated in the SDFs. Figure 7 presents the SDF for syringic acid and 1,2-butanediol at a hydrotrope mole percentage of 20 or 80%. SDFs were obtained using the program TRAVIS.[89,90] It is evident that syringic acid is solvated by the alkyl chain of the hydrotrope around the aromatic ring. In contrast, water molecules are primarily located near the oxygen atoms of both the hydrotrope and solute molecules. Interestingly, the primary difference observed at varying hydrotrope concentrations is the spatial positioning of the hydrotrope molecules. At low hydrotrope concentrations, it is clear that these molecules interact primarily among themselves via the alkyl chain. Conversely, at high hydrotrope concentrations, where water no longer serves as the principal solvent within the mixtures, the hydrotrope molecules compete with water in the solvation of oxygen atoms, whether located in the solute or within the hydrotrope itself.

Coordination Number Analysis. The coordination number (CN) quantifies the subtle differences observed in the RDFs. Figure 8 shows the coordination number of carbon

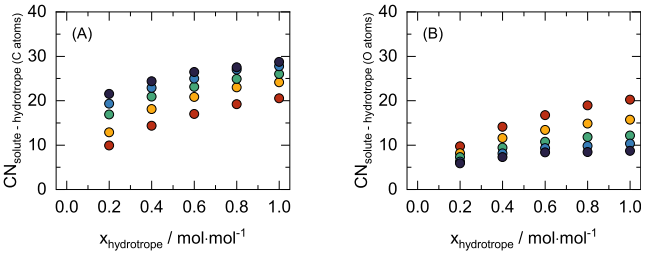

Figure 8. Coordination number (CN) at a distance of 0.65 nm between the center of mass of syringic acid and the carbon atoms (A) or oxygen atoms (B) of the hydrotrope. Hydrotropes: 1,2-ethanediol (●), 1,2-propanediol (●), 1,2-butanediol (●), 1,2-pentanediol (●), and 1,2-hexanediol (●).

(A) and oxygen atoms (B) around syringic acid at a distance of 0.65 nm, which corresponds to the first minimum in the RDFs (Figure 6). As the hydrotrope concentration increases, the number of atoms around the solute increases, though this effect is more pronounced at lower hydrotrope concentrations, where the interactions between the solute and the hydrotrope are stronger.

Two additional trends are evident: Figure 8A shows that as the alkyl chain length increases, the population of carbon atoms around the solute increases, due to the higher proportion of carbon atoms in the mixture. However, Figure 8B illustrates a different trend for oxygen atoms, where their coordination around the solute decreases with longer alkyl chains. This is attributed to steric effects, as longer chains

https://doi.org/10.1021/acs.jpcb.5c01542
J. Phys. Chem. B XXXX, XXX, XXX−XXX

hinder the accommodation of hydroxyl groups around the solute.

Another steric effect is observed in the accommodation of carbon atoms around the solute; although 1,2-hexanediol has more carbon atoms than 1,2-pentanediol, their coordination numbers are similar at high hydrotrope content. This supports the idea that hydrophobic interactions between the hydrotrope and the solute are maximized when the volume of their nonpolar regions are the same,[34] making it more challenging for longer alkyl chain hydrotropes to accommodate around the solute.

Hydrogen Bonds Analysis. It is known that hydrogen bonds are not the driving force for hydrotropy; however, they reinforce the structuring of the solute−solvent system.[91] Figure 9 shows the number of hydrogen bonds per solute molecule,

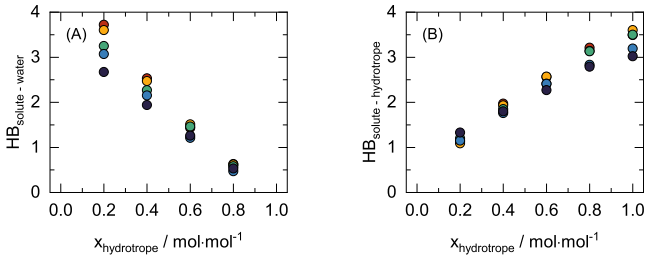

Figure 9. Hydrogen bonds (HB) between syringic acid and water (A) and syringic acid and hydrotrope (B) per solutes molecules. Hydrotropes: 1,2-ethanediol (●), 1,2-propanediol (●), 1,2-butanediol (●), 1,2-pentanediol (●), and 1,2-hexanediol (●).

encompassing both solute-water and solute-hydrotrope interactions, across a range of hydrotrope concentrations. Hydrogen bonds were computed in GROMACS based on the geometrical criteria of a donor−acceptor distance of 0.35 nm or less and a hydrogen-donor−acceptor angle of 30° or less. When water molecules are the primary solvent in the mixture, solutes capable of forming hydrogen bonds will preferentially bond with water molecules. As a result, hydrotropes do not primarily interact through hydrogen bonding with the solute. This is the reason why hydrotrope molecules were not found mainly around the oxygen atoms of the solute and hydrotrope in SDFs with a low hydrotrope content (Figure 7A,C). However, at high hydrotrope content, which means a low water content, the hydrotrope molecules compete with the water molecules to form hydrogen bonds with the solute and the hydrotrope molecules can be found around the same places as the water molecules (Figure 7B,D).

The effect of the alkyl chain length on hydrogen bond formation is opposite to the hydrophobic interactions discussed in the previous sections. Figure 9A depicts the hydrogen bond formation between water and solute, with the main differences observable at high water content. The alkyl chain of the hydrotrope hinders the accommodation of water molecules for hydrogen bond formation due to the steric effect caused by the presence of its hydrophobic part around the solute. For this reason, 1,2-ethanediol can allow more water molecules around the solute to form hydrogen bonds than 1,2-hexanediol. Figure 9B shows the same effect on hydrogen bond formation between solute and hydrotrope, which can be observed at high hydrotrope content (low water content).

Interestingly, this trend in hydrogen bond formation was also observed in the experimental solubility at high hydrotrope content. For those hydrotropes with the worst performance in hydrogen bond formation, the addition of water increases the solubility in the same way that it increases the hydrogen bond formation of solute-water. This indicates that at high hydrotrope content, the driving force for the aggregation of solvent molecules around the solute is not the hydrophobic interaction observed at low concentrations, but rather the hydrogen bond capabilities. This aligns with the different trends observed at each end of the experimental solubility spectrum, as well as previous observations using cyrene.[9]

CONCLUSIONS

MD simulations elucidated the mechanism by which 1,2-alkanediols act as hydrotropes to enhance the syringic acid solubility in water. The key interactions influencing solubility were found to be those between the solute and the hydrotrope, as well as those between the solute and water, which vary with the presence of the hydrotrope. Using KBI analysis, these interactions could be quantified and related to changes in the solute chemical potential. MD simulations revealed that at low hydrotrope concentrations, all studied 1,2-alkanediols exhibit a higher affinity for the solute-hydrotrope interaction compared to the solute-water interaction. This affinity increases with the alkyl chain length, suggesting that longer alkyl chains contribute more significantly to the hydrotrope aggregation around the solute. This observation is corroborated by RDF and SDF analyses, which demonstrated that syringic acid predominantly associates with the hydrotrope alkyl chains, while the hydrotrope tends to surround the apolar regions of the solute. These findings support the hypothesis that hydrophobic interactions are the primary driving force behind the hydrotropic effect.

At high hydrotrope concentrations, changes occur in the affinity of the solute for the hydrotrope compared to water. This effect is particularly pronounced for hydrotropes with longer alkyl chains, leading to a decrease in solubility as the hydrotrope concentration increases. In other words, the water addition can paradoxically enhance the hydrophobic solute solubility in these systems. In regions of excess hydrotrope, water ceases to be the primary solvent, resulting in a reduction of the hydrogen bonding that reinforces the solute−solvent structure. Consequently, the hydrotrope molecules must compensate for this loss of hydrogen bonding. Longer alkyl chain hydrotropes are less efficient in this regard due to steric effects that hinder their ability to form hydrogen bonds effectively.

ASSOCIATED CONTENT

Data Availability Statement

Additionally, the analysis code for KBI calculation is available to the public at https://github.com/MaginnGroup/syringic_acid_KBI, including example GROMACS files along with the force field parameters for each molecule used in this work.

Supporting Information

The Supporting Information is available free of charge at https://pubs.acs.org/doi/10.1021/acs.jpcb.5c01542.

The number of molecules and simulation times for each system. AARD for the pure density of each hydrotrope. Additional figures for RDFs (PDF)

https://doi.org/10.1021/acs.jpcb.5c01542
J. Phys. Chem. B XXXX, XXX, XXX−XXX

AUTHOR INFORMATION

Corresponding Author

Edward J. Maginn − *Department of Chemical and Biomolecular Engineering, University of Notre Dame, Notre Dame, Indiana 46556, United States;* orcid.org/0000-0002-6309-1347; Email: ed@nd.edu

Authors

Esteban Cea-Klapp − *Departamento de Ingeniería Química, Universidad de Concepción, Concepción 4070386, Chile; Department of Chemical and Biomolecular Engineering, University of Notre Dame, Notre Dame, Indiana 46556, United States;* orcid.org/0000-0002-3571-4973

Dinis O. Abranches − *CICECO − Aveiro Institute of Materials, Department of Chemistry, University of Aveiro, Aveiro 3810-193, Portugal;* orcid.org/0000-0003-0097-2072

Eliseo Marin-Rimoldi − *Department of Chemical and Biomolecular Engineering, University of Notre Dame, Notre Dame, Indiana 46556, United States*

Nicolás F. Gajardo-Parra − *Departamento de Ingeniería Química y Bioprocesos, Pontificia Universidad Católica de Chile, Santiago 7820436, Chile*

Roberto I. Canales − *Departamento de Ingeniería Química y Bioprocesos, Pontificia Universidad Católica de Chile, Santiago 7820436, Chile*

José Matías Garrido − *Departamento de Ingeniería Química, Universidad de Concepción, Concepción 4070386, Chile;* orcid.org/0000-0001-9989-7206

Complete contact information is available at: https://pubs.acs.org/10.1021/acs.jpcb.5c01542

Notes

The authors declare no competing financial interest.

ACKNOWLEDGMENTS

This work has been financed by FONDECYT, Chile (Project 1230236 and 1240765). Esteban Cea-Klapp's work was funded by the National Agency for Research and Development (ANID)/Scholarship Program/DOCTORADO BECA NACIONAL/2021-21210786. This work was partly funded by the project CICECO Aveiro Institute of Materials, UIDB/50011/2020, UIDP/50011/2020, and LA/P/0006/2020, financed by Portuguese funds through the FCT/MCTES (PIDDAC). We acknowledge the support of the Seed Fund provided by the School of Engineering at Pontificia Universidad Católica de Chile. This research was supported by computing resources from the Center for Research Computing (CRC) at the University of Notre Dame.

REFERENCES

(1) Neuberg, C. Hydrotropische Erscheinungen. *Biochem. Z.* **1916**, *76*, 107.

(2) Mehringer, J.; Kunz, W. Carl Neuberg's hydrotropic appearances (1916). *Adv. Colloid Interface Sci.* **2021**, *294*, No. 102476.

(3) Eastoe, J.; Hatzopoulos, M. H.; Dowding, P. J. Action of hydrotropes and alkyl-hydrotropes. *Soft Matter* **2011**, *7*, 5917−5925.

(4) Kunz, W.; Holmberg, K.; Zemb, T. Hydrotropes. *Curr. Opin. Colloid Interface Sci.* **2016**, *22*, 99−107.

(5) Patel, A. D.; Desai, M. A. Progress in the field of hydrotropy: mechanism, applications and green concepts. *Reviews in Chemical Engineering* **2023**, *39*, 601−630.

(6) Janicka, P.; Płotka-Wasylka, J.; Jatkowska, N.; Chabowska, A.; Fares, M. Y.; Andruch, V.; Kaykhaii, M.; Gębicki, J. Trends in the new generation of green solvents in extraction processes. *Curr. Opin. Green Sustainable Chem.* **2022**, *37*, No. 100670.

(7) Abranches, D. O.; Benfica, J.; Shimizu, S.; Coutinho, J. A. P. The Perspective of Cooperative Hydrotropy on the Solubility in Aqueous Solutions of Cyrene. *Ind. Eng. Chem. Res.* **2020**, *59*, 18649−18658.

(8) Bruyn, M. D.; Budarin, V. L.; Misefari, A.; Shimizu, S.; Fish, H.; Cockett, M.; Hunt, A. J.; Hofstetter, H.; Weckhuysen, B. M.; Clark, J. H.; et al. Geminal Diol of Dihydrolevoglucosenone as a Switchable Hydrotrope: A Continuum of Green Nanostructured Solvents. *ACS Sustainable Chem. Eng.* **2019**, *7*, 7878−7883.

(9) Abranches, D. O.; Benfica, J.; Shimizu, S.; Coutinho, J. A. P. Solubility Enhancement of Hydrophobic Substances in Water/Cyrene Mixtures: A Computational Study. *Ind. Eng. Chem. Res.* **2020**, *59*, 18247−18253.

(10) Silva, S. S.; Abranches, D. O.; Pinto, A. S.; Soares, B. P.; Passos, H.; Ferreira, A. M.; Coutinho, J. A. P. Solubility Enhancement of Hydrophobic Compounds in Aqueous Solutions Using Biobased Solvents as Hydrotropes. *Ind. Eng. Chem. Res.* **2023**, *62*, 12021−12028.

(11) Soares, B. P.; Abranches, D. O.; Sintra, T. E.; Leal-Duaso, A.; García, J. I.; Pires, E.; Shimizu, S.; Pinho, S. P.; Coutinho, J. A. P. Glycerol Ethers as Hydrotropes and Their Use to Enhance the Solubility of Phenolic Acids in Water. *ACS Sustainable Chem. Eng.* **2020**, *8*, 5742−5749.

(12) Abranches, D. O.; Soares, B. P.; Ferreira, A. M.; Shimizu, S.; Pinho, S. P.; Coutinho, J. A. P. The impact of size and shape in the performance of hydrotropes: a case-study of alkanediols. *Phys. Chem. Chem. Phys.* **2022**, *24*, 7624−7634.

(13) Sintra, T. E.; Abranches, D. O.; Benfica, J.; Soares, B. P.; Ventura, S. P.; Coutinho, J. A. Cholinium-based ionic liquids as bioinspired hydrotropes to tackle solubility challenges in drug formulation. *Eur. J. Pharm. Biopharm.* **2021**, *164*, 86−92.

(14) Sintra, T. E.; Shimizu, K.; Ventura, S. P. M.; Shimizu, S.; Lopes, J. N. C.; Coutinho, J. A. P. Enhanced dissolution of ibuprofen using ionic liquids as catanionic hydrotropes. *Phys. Chem. Chem. Phys.* **2017**, *20*, 2094−2103.

(15) Sales, I.; Abranches, D.; Sintra, T. E.; Mattedi, S.; Freire, M. G.; Coutinho, J. A.; Pinho, S. P. Selection of hydrotropes for enhancing the solubility of artemisinin in aqueous solutions. *Fluid Phase Equilib.* **2022**, *562*, No. 113556.

(16) Cláudio, A. F. M.; Neves, M. C.; Shimizu, K.; Lopes, J. N. C.; Freire, M. G.; Coutinho, J. A. P. The magic of aqueous solutions of ionic liquids: ionic liquids as a powerful class of catanionic hydrotropes. *Green Chem.* **2015**, *17*, 3948−3963.

(17) Sosa, F. H. B.; Abranches, D. O.; Lopes, A. M. D. C.; Costa, M. C. D.; Coutinho, J. A. P. Role of Deep Eutectic Solvent Precursors as Hydrotropes: Unveiling Synergism/Antagonism for Enhanced Kraft Lignin Dissolution. *ACS Sustainable Chem. Eng.* **2024**, *12*, 8930−8940.

(18) Badwan, A.; El-Khordagui, L.; Saleh, A.; Khalil, S. The solubility of benzodiazepines in sodium salicylate solution and a proposed mechanism for hydrotropic solubilization. *Int. J. Pharm.* **1982**, *13*, 67−74.

(19) Balasubramanian, D.; Srinivas, V.; Gaikar, V. G.; Sharma, M. M. Aggregation behavior of hydrotropic compounds in aqueous solution. *J. Phys. Chem.* **1989**, *93*, 3865−3870.

(20) Silva, R. C. D.; Spitzer, M.; Silva, L. H. D.; Loh, W. Investigations on the mechanism of aqueous solubility increase caused by some hydrotropes. *Thermochim. Acta* **1999**, *328*, 161−167.

(21) Bauduin, P.; Renoncourt, A.; Kopf, A.; Touraud, D.; Kunz, W. Unified Concept of Solubilization in Water by Hydrotropes and Cosolvents. *Langmuir* **2005**, *21*, 6769−6775.

(22) Patel, A. D.; Desai, M. A. Aggregation Behavior and Thermodynamic Studies of Hydrotropes: A Review. *Tenside Surfactants Detergents* **2020**, *57*, 192−202.

(23) Frank, H. S.; Franks, F. Structural Approach to the Solvent Power of Water for Hydrocarbons; Urea as a Structure Breaker. *J. Chem. Phys.* **1968**, *48*, 4746−4757.
(24) Coffman, R. E.; Kildsig, D. O. Effect of nicotinamide and urea on the solubility of riboflavin in various solvents. *J. Pharm. Sci.* **1996**, *85*, 951−954.
(25) Sanghvi, R.; Evans, D.; Yalkowsky, S. H. Stacking complexation by nicotinamide: A useful way of enhancing drug solubility. *Int. J. Pharm.* **2007**, *336*, 35−41.
(26) Cui, Y. Parallel stacking of caffeine with riboflavin in aqueous solutions: The potential mechanism for hydrotropic solubilization of riboflavin. *Int. J. Pharm.* **2010**, *397*, 36−43.
(27) Das, S.; Paul, S. Hydrotropic Action of Cationic Hydrotrope p-Toluidinium Chloride on the Solubility of Sparingly Soluble Gliclazide Drug Molecule: A Computational Study. *J. Chem. Inf. Model.* **2017**, *57*, 1461−1473.
(28) Das, S.; Paul, S. Hydrotropic Solubilization of Sparingly Soluble Riboflavin Drug Molecule in Aqueous Nicotinamide Solution. *J. Phys. Chem. B* **2017**, *121*, 8774−8785.
(29) Das, S.; Paul, S. Computer Simulation Studies of the Mechanism of Hydrotrope-Assisted Solubilization of a Sparingly Soluble Drug Molecule. *J. Phys. Chem. B* **2016**, *120*, 3540−3550.
(30) Das, S.; Paul, S. Mechanism of Hydrotropic Action of Hydrotrope Sodium Cumene Sulfonate on the Solubility of Di-t-Butyl-Methane: A Molecular Dynamics Simulation Study. *J. Phys. Chem. B* **2016**, *120*, 173−183.
(31) Booth, J. J.; Abbott, S.; Shimizu, S. Mechanism of Hydrophobic Drug Solubilization by Small Molecule Hydrotropes. *J. Phys. Chem. B* **2012**, *116*, 14915−14921.
(32) Booth, J. J.; Omar, M.; Abbott, S.; Shimizu, S. Hydrotrope accumulation around the drug: the driving force for solubilization and minimum hydrotrope concentration for nicotinamide and urea. *Phys. Chem. Chem. Phys.* **2015**, *17*, 8028−8037.
(33) Shimizu, S.; Matubayasi, N. The origin of cooperative solubilisation by hydrotropes. *Phys. Chem. Chem. Phys.* **2016**, *18*, 25621−25628.
(34) Abranches, D. O.; Benfica, J.; Soares, B. P.; Leal-Duaso, A.; Sintra, T. E.; Pires, E.; Pinho, S. P.; Shimizu, S.; Coutinho, J. A. P. Unveiling the mechanism of hydrotropy: evidence for water-mediated aggregation of hydrotropes around the solute. *Chem. Commun.* **2020**, *56*, 7143−7146.
(35) Berendsen, H. J. C.; Grigera, J. R.; Straatsma, T. P. The missing term in effective pair potentials. *J. Phys. Chem.* **1987**, *91*, 6269−6271.
(36) Wang, J.; Wolf, R. M.; Caldwell, J. W.; Kollman, P. A.; Case, D. A. Development and testing of a general amber force field. *J. Comput. Chem.* **2004**, *25*, 1157−1174.
(37) Wang, J.; Wang, W.; Kollman, P. A.; Case, D. A. Automatic atom type and bond type perception in molecular mechanical calculations. *Journal of Molecular Graphics and Modelling* **2006**, *25*, 247−260.
(38) Silva, A. W. S. D.; Vranken, W. F. ACPYPE - AnteChamber PYthon Parser interfacE. *BMC Res. Notes* **2012**, *5*, 367.
(39) Lorentz, H. A. Ueber die Anwendung des Satzes vom Virial in der kinetischen Theorie der Gase. *Annalen der Physik* **1881**, *248*, 127−136.
(40) Berthelot, D. Hebd. *Seances Acad. Sci.* **1898**, *126*, 1703.
(41) Schauperl, M.; Nerenberg, P. S.; Jang, H.; Wang, L.-P.; Bayly, C. I.; Mobley, D. L.; Gilson, M. K. Non-bonded force field model with advanced restrained electrostatic potential charges (RESP2). *Commun. Chem.* **2020**, *3*, 44.
(42) Miertuš, S.; Scrocco, E.; Tomasi, J. Electrostatic interaction of a solute with a continuum. A direct utilizaion of AB initio molecular potentials for the prevision of solvent effects. *Chem. Phys.* **1981**, *55*, 117−129.
(43) Mennucci, B.; Cancès, E.; Tomasi, J. Evaluation of Solvent Effects in Isotropic and Anisotropic Dielectrics and in Ionic Solutions with a Unified Integral Equation Method: Theoretical Bases, Computational Implementation, and Numerical Applications. *J. Phys. Chem. B* **1997**, *101*, 10506−10517.
(44) Frisch, M. J.; Trucks, G. W.; Schlegel, H. B.; Scuseria, G. E.; Robb, M. A.; Cheeseman, J. R.; Scalmani, G.; Barone, V.; Petersson, G. A.; Nakatsuji, H. et al. *Gaussian 16 Revision C.01*; Gaussian Inc.: Wallingford, CT, 2016. https://gaussian.com/gaussian16/.
(45) Kelly, B. D.; Smith, W. R. A Simple Method for Including Polarization Effects in Solvation Free Energy Calculations When Using Fixed-Charge Force Fields: Alchemically Polarized Charges. *ACS Omega* **2020**, *5*, 17170−17181.
(46) Weerasinghe, S.; Smith, P. E. A Kirkwood-Buff Derived Force Field for Mixtures of Urea and Water. *J. Phys. Chem. B* **2003**, *107*, 3891−3898.
(47) Berendsen, H.; Spoel, D. V. D.; Drunen, R. V. GROMACS: A message-passing parallel molecular dynamics implementation. *Comput. Phys. Commun.* **1995**, *91*, 43−56.
(48) Abraham, M. J.; Murtola, T.; Schulz, R.; Páll, S.; Smith, J. C.; Hess, B.; Lindahl, E. GROMACS: High performance molecular simulations through multi-level parallelism from laptops to supercomputers. *SoftwareX* **2015**, *1*, 19−25.
(49) Cuendet, M. A.; van Gunsteren, W. F. On the calculation of velocity-dependent properties in molecular dynamics simulations using the leapfrog integration algorithm. *J. Chem. Phys.* **2007**, *127*, 184102.
(50) Darden, T.; York, D.; Pedersen, L. Particle mesh Ewald: An N · log(N) method for Ewald sums in large systems. *J. Chem. Phys.* **1993**, *98*, 10089−10092.
(51) Hess, B.; Bekker, H.; Berendsen, H. J. C.; Fraaije, J. G. E. M. LINCS: A linear constraint solver for molecular simulations. *J. Comput. Chem.* **1997**, *18*, 1463−1472.
(52) Martínez, L.; Andrade, R.; Birgin, E. G.; Martínez, J. M. PACKMOL: A package for building initial configurations for molecular dynamics simulations. *J. Comput. Chem.* **2009**, *30*, 2157−2164.
(53) Bussi, G.; Donadio, D.; Parrinello, M. Canonical sampling through velocity rescaling. *J. Chem. Phys.* **2007**, *126*, No. 014101.
(54) Berendsen, H. J. C.; Postma, J. P. M.; van Gunsteren, W. F.; DiNola, A.; Haak, J. R. Molecular dynamics with coupling to an external bath. *J. Chem. Phys.* **1984**, *81*, 3684−3690.
(55) Nosé, S. A molecular dynamics method for simulations in the canonical ensemble. *Mol. Phys.* **1984**, *52*, 255−268.
(56) Hoover, W. G. Canonical dynamics: Equilibrium phase-space distributions. *Phys. Rev. A* **1985**, *31*, 1695−1697.
(57) Parrinello, M.; Rahman, A. Polymorphic transitions in single crystals: A new molecular dynamics method. *J. Appl. Phys.* **1981**, *52*, 7182−7190.
(58) Nosé, S.; Klein, M. Constant pressure molecular dynamics for molecular systems. *Mol. Phys.* **1983**, *50*, 1055−1076.
(59) Kirkwood, J. G.; Buff, F. P. The Statistical Mechanical Theory of Solutions. *I. The Journal of Chemical Physics* **1951**, *19*, 774−777.
(60) Kang, M.; Smith, P. E. Kirkwood−Buff theory of four and higher component mixtures. *J. Chem. Phys.* **2008**, *128*, 244511.
(61) Ben-Naim, A. Inversion of the Kirkwood−Buff theory of solutions: Application to the water−ethanol system. *J. Chem. Phys.* **1977**, *67*, 4884−4890.
(62) Dawass, N.; Krüger, P.; Schnell, S. K.; Simon, J.-M.; Vlugt, T. Kirkwood-Buff integrals from molecular simulation. *Fluid Phase Equilib.* **2019**, *486*, 21−36.
(63) Krüger, P.; Schnell, S. K.; Bedeaux, D.; Kjelstrup, S.; Vlugt, T. J. H.; Simon, J.-M. Kirkwood−Buff Integrals for Finite Volumes. *J. Phys. Chem. Lett.* **2013**, *4*, 235−238.
(64) Sugita, Y.; Okamoto, Y. Replica-exchange multicanonical algorithm and multicanonical replica-exchange method for simulating systems with rough energy landscape. *Chem. Phys. Lett.* **2000**, *329*, 261−270.
(65) Bussi, G. Hamiltonian replica exchange in GROMACS: a flexible implementation. *Mol. Phys.* **2014**, *112*, 379−384.
(66) Metropolis, N.; Rosenbluth, A. W.; Rosenbluth, M. N.; Teller, A. H.; Teller, E. Equation of State Calculations by Fast Computing Machines. *J. Chem. Phys.* **1953**, *21*, 1087−1092.

https://doi.org/10.1021/acs.jpcb.5c01542
J. Phys. Chem. B XXXX, XXX, XXX−XXX

(67) Beutler, T. C.; Mark, A. E.; Schaik, R. C. V.; Gerber, P. R.; Gunsteren, W. F. V. Avoiding singularities and numerical instabilities in free energy calculations based on molecular simulations. *Chem. Phys. Lett.* **1994**, *222*, 529−539.
(68) Shirts, M. R.; Chodera, J. D. Statistically optimal analysis of samples from multiple equilibrium states. *J. Chem. Phys.* **2008**, *129*, 124105.
(69) Klimovich, P. V.; Shirts, M. R.; Mobley, D. L. Guidelines for the analysis of free energy calculations. *J. Comput. Aided Mol. Des* **2015**, *29*, 397−411.
(70) Skylogianni, E.; Wanderley, R. R.; Austad, S. S.; Knuutila, H. K. Density and Viscosity of the Nonaqueous and Aqueous Mixtures of Methyldiethanolamine and Monoethylene Glycol at Temperatures from 283.15 to 353.15 K. *J. Chem. Eng. Data* **2019**, *64* (12), 5415−5431.
(71) Tsierkezos, N. G.; Palaiologou, M. M. Ultrasonic studies of liquid mixtures of either water or dimethylsulfoxide with ethylene glycol, diethylene glycol, triethylene glycol, tetraethylene glycol, 1,2-propylene glycol and 1,4-butylene glycol at 298.15 K. *Phys. Chem. Liq.* **2009**, *47*, 447−459.
(72) Sagdeev, D.; Fomina, M.; Alyaev, V.; Musin, R.; Abdulagatov, I. Density of Working Liquids for Diffusion Vacuum Pumps. *J. Chem. Eng. Data* **2018**, *63* (5), 1698−1705.
(73) Chang, C.-W.; Hsiung, T.-L.; Lui, C.-P.; Tu, C.-H. Densities, surface tensions, and isobaric vapor−liquid equilibria for the mixtures of 2-propanol, water, and 1,2-propanediol. *Fluid Phase Equilib.* **2015**, *389*, 28−40.
(74) Atilhan, M.; Aparicio, S. PρT measurements and derived properties of liquid 1,2-alkanediols. *J. Chem. Thermodyn.* **2013**, *57*, 137−144.
(75) Checoni, R. F. Experimental study of the excess molar volume of ternary mixtures containing {water+(1,2-propanediol, or 1,3-propanediol, or 1,2-butanediol, or 1,3-butanediol, or 1,4-butanediol, or 2,3-butanediol)+electrolytes} at a temperature of 298.15K and atmospheric pressure. *J. Chem. Thermodyn.* **2010**, *42*, 612−620.
(76) Parsa, J. B.; Haghro, M. F. Excess molar volume and viscosity deviation for binary mixtures of polyethylene glycol dimethyl ether 250 with 1,2-alkanediols (C3−C6) at T = (293.15 to 323.15)K. *J. Chem. Thermodyn.* **2008**, *40* (5), 782−788.
(77) Piekarski, H.; Pietrzak, A. Molecular interactions of alkanediols in methanol and in water: density and heat capacity measurements. *J. Mol. Liq.* **2005**, *121*, 46−52.
(78) Zemánková, K.; Troncoso, J.; Romaní, L. Excess volumes and excess heat capacities for alkanediol+water systems in the temperature interval (283.15−313.15)K. *Fluid Phase Equilib.* **2013**, *356*, 1−10.
(79) Romero, C. M.; Páez, M. S.; Arteaga, J. C.; Romero, M. A.; Negrete, F. Effect of temperature on the volumetric properties of dilute aqueous solutions of 1,2-hexanediol, 1,5-hexanediol, 1,6-hexanediol, and 2,5-hexanediol. *J. Chem. Thermodyn.* **2007**, *39*, 1101−1109.
(80) Egorov, G. I.; Makarov, D. M.; Kolker, A. M. Volumetric properties of the water-ethylene glycol mixtures in the temperature range 278−333.15 K at atmospheric pressure. *Russian Journal of General Chemistry* **2010**, *80*, 1577−1585.
(81) Parsons, M. T.; Lau, F. W.; Yee, E. G.; Koga, Y. Excess Chemical Potentials and Partial Molar Enthalpies in Aqueous 1,2- and 1,3-Propanediols at 25°C. *J. Solution Chem.* **2003**, *32*, 137−153.
(82) Huot, J.-Y.; Battistel, E.; Lumry, R.; Villeneuve, G.; Lavallee, J.-F.; Anusiem, A.; Jolicoeur, C. A comprehensive thermodynamic investigation of water-ethylene glycol mixtures at 5, 25, and 45°C. *J. Solution Chem.* **1988**, *17*, 601−636.
(83) Makarov, D. M.; Egorov, G. I.; Markarian, S. A.; Kolker, A. M. Excess Gibbs Energy and Local Compositions in the Mixtures C2, C3 Alkane Diols and Triols with Water at Various Pressures. *J. Solution Chem.* **2016**, *45*, 1679−1688.
(84) Perera, A.; Sokolić, F.; Almásy, L.; Koga, Y. Kirkwood-Buff integrals of aqueous alcohol binary mixtures. *J. Chem. Phys.* **2006**, *124*, 124515.
(85) Paluch, A. S.; Cryan, D. D.; Maginn, E. J. Predicting the Solubility of the Sparingly Soluble Solids 1,2,4,5-Tetramethylbenzene, Phenanthrene, and Fluorene in Various Organic Solvents by Molecular Simulation. *Journal of Chemical & Engineering Data* **2011**, *56*, 1587−1595.
(86) Paluch, A. S.; Parameswaran, S.; Liu, S.; Kolavennu, A.; Mobley, D. L. Predicting the excess solubility of acetanilide, acetaminophen, phenacetin, benzocaine, and caffeine in binary water/ethanol mixtures via molecular simulation. *J. Chem. Phys.* **2015**, *142*, No. 044508.
(87) Smith, P. E. Chemical Potential Derivatives and Preferential Interaction Parameters in Biological Systems from Kirkwood-Buff Theory. *Biophys. J.* **2006**, *91*, 849−856.
(88) Shimizu, S.; Matubayasi, N. Unifying hydrotropy under Gibbs phase rule. *Phys. Chem. Chem. Phys.* **2017**, *19*, 23597−23605.
(89) Brehm, M.; Kirchner, B. TRAVIS - A Free Analyzer and Visualizer for Monte Carlo and Molecular Dynamics Trajectories. *J. Chem. Inf. Model.* **2011**, *51*, 2007−2023.
(90) Brehm, M.; Thomas, M.; Gehrke, S.; Kirchner, B. TRAVIS—A free analyzer for trajectories from molecular simulation. *J. Chem. Phys.* **2020**, *152*, 164105.
(91) Hahn, M.; Krickl, S.; Buchecker, T.; Jošt, G.; Touraud, D.; Bauduin, P.; Pfitzner, A.; Klamt, A.; Kunz, W. Ab initio prediction of structuring/mesoscale inhomogeneities in surfactant-free microemulsions and hydrogen-bonding-free microemulsions. *Phys. Chem. Chem. Phys.* **2019**, *21*, 8054−8066.

https://doi.org/10.1021/acs.jpcb.5c01542
J. Phys. Chem. B XXXX, XXX, XXX−XXX